Toward a MILP Modeling Framework for Distribution System Restoration

Bo Chen, *Member, IEEE*, Zhigang Ye, *Student Member, IEEE*, Chen Chen, *Member, IEEE*, Jianhui Wang, *Senior Member, IEEE*

***Abstract*—Large-scale blackouts and extreme weather events in recent decades raise the concern for improving the resilience of electric power infrastructures. Distribution service restoration (DSR), a fundamental application in outage management systems (OMS), provides restoration solutions for system operators when power outages happen. As distribution generators (DGs) and remotely controllable devices are increasingly installed in distribution systems, an advanced DSR framework is needed to perform optimally coordinated restoration that can achieve maximal restoration performance. This paper introduces a DSR modeling framework, which can generate optimal switching sequences and estimated time of restoration (ETR) in the presence of remotely controllable switches, manually operated switches, and dispatchable DGs. Two mathematical models, a variable time step (VTS) model and a fixed time step (FTS) model, are presented and compared. The proposed models are formulated as a mixed-integer linear programming (MILP) model, and their effectiveness is evaluated via the IEEE 123 node test feeder.**

***Index Terms*—Distribution system, distributed generation, mixed-integer linear programming, service restoration, switching sequence management**

NOMENCLATURE

Sets

$\mathcal{N}$	Set of nodes
$\mathcal{B}$	Set of branches
$\mathcal{G}$	Set of DGs and substations
$\mathcal{L}$	Set of loads
$\mathcal{V}$	Set of regulators
$\mathcal{C}$	Set of node cells
$\mathcal{B}^S$	Set of switchable branches
$\mathcal{B}^F$	Set of branches in failure status
$\mathcal{G}^S$	Set of black-start DGs/substations
$\mathcal{G}^F$	Set of DGs/substations in failure status
$\mathcal{L}^S$	Set of switchable loads
$\mathcal{L}^F$	Set of loads in failure status
$\mathcal{T}$	Set of time steps for FTS model
$\mathcal{P}$	Set of check points for VTS model

Parameters

T_{ij}^R	Travel time for an energization agent to travel from node cell $C_i \in \mathcal{C}$ to $C_j \in \mathcal{C}$.
T_{ii}^R	Starting time for an energization agent starts to travel from node cell $C_i \in \mathcal{C}$.
T^{Rmax}	Maximum restoration time.
$\tilde{\boldsymbol{z}}_{ij} \in \mathbb{C}^{3\times3}$	Modified three-phase line impedance matrix of branch $(i,j) \in \mathcal{B}\backslash\mathcal{V}$.
$\boldsymbol{e}_{ij}^{\phi} \in \{0,1\}^{3\times1}$	Phase indicator vector of branch $(i,j) \in \mathcal{B}\backslash\mathcal{V}$.
P_g^{max}	Maximum active output power of DG $g \in \mathcal{G}$.
P_g^{min}	Minimum active output power of DG $g \in \mathcal{G}$.
Q_g^{max}	Maximum reactive output power of DG $g \in \mathcal{G}$.
Q_g^{min}	Minimum reactive output power of DG $g \in \mathcal{G}$.
$\boldsymbol{P}_{ij}^{max} \in \mathbb{R}^{3\times1}$	Maximum three-phase active power capacity of branch $(i,j) \in \mathcal{B}$.
$\boldsymbol{Q}_{ij}^{max} \in \mathbb{R}^{3\times1}$	Maximum three-phase reactive power capacity of branch $(i,j) \in \mathcal{B}$.
$\boldsymbol{U}^{max} \in \mathbb{R}^{3\times1}$	Maximum squared three-phase nodal voltage.
$\boldsymbol{U}^{min} \in \mathbb{R}^{3\times1}$	Minimum squared three-phase nodal voltage.
$\boldsymbol{\beta}_{ij}^{max} \in \mathbb{R}^{3\times1}$	Maximum squared three-phase ratio of regulator $(i,j) \in \mathcal{V}$.
$\boldsymbol{\beta}_{ij}^{min} \in \mathbb{R}^{3\times1}$	Minimum squared three-phase ratio of regulator $(i,j) \in \mathcal{V}$.
ω_l^L	Weighting factor of load $l \in \mathcal{L}$.
M	A large positive value.

Variables

Decision Variables

$x_{ij,t}^B$	Binary variable to indicate if branch $(i,j) \in \mathcal{B}$ is energized at check point $t \in \mathcal{P}$ for VTS model or time step $t \in \mathcal{T}$ for FTS model.
$x_{l,t}^L$	Binary to indicate if load $l \in \mathcal{L}$ is energized at $t \in \mathcal{P}$ or $t \in \mathcal{T}$.
$x_{g,t}^G$	Binary to indicate if substation/DG $g \in \mathcal{G}$ is energized at $t \in \mathcal{P}$ or $t \in \mathcal{T}$.
x_{ij}^R	Binary to indicate if there is a virtual energization agent that travels from node cell $C_i \in \mathcal{C}$ to $C_j \in \mathcal{C}$.
$\boldsymbol{P}_{g,t}^G \in \mathbb{R}^{3\times1}$	Three-phase active power output of DG $g \in \mathcal{G}$ at $t \in \mathcal{P}$ or $t \in \mathcal{T}$.
$\boldsymbol{Q}_{g,t}^G \in \mathbb{R}^{3\times1}$	Three-phase reactive power output of DG $g \in \mathcal{G}$ at $t \in \mathcal{P}$ or $t \in \mathcal{T}$.
$\boldsymbol{\beta}_{ij,t} \in \mathbb{R}^{3\times1}$	Squared three-phase ratio of regulator $(i,j) \in \mathcal{V}$ at $t \in \mathcal{P}$ or $t \in \mathcal{T}$.

The work of B. Chen, C. Chen, and J. Wang was supported by the U.S. Department of Energy's Solar Energy Technologies Office.

B. Chen and C. Chen are with the Energy Systems Division, Argonne National Laboratory, Argonne, IL 60439 USA (e-mail: bo.chen@anl.gov, morningchen@anl.gov).

Z. Ye is with the State Key Laboratory of Electrical Insulation and Power Equipment, Xi'an Jiaotong University, Xi'an, Shaanxi, 710049, China, and the Energy Systems Division, Argonne National Laboratory, Argonne, IL 60439 USA (e-mail: yzhg.2009@stu.xjtu.edu.cn, zhigang.ye@anl.gov)

J. Wang is with the Department of Electrical Engineering at Southern Methodist University, Dallas, TX, USA (email: jianhui@mail.smu.edu)

State Variables

t_i	Time when an energization agent arrives at node cell $C_i \in \mathcal{C}$.
$s^C_{C_i,t}$	Binary to indicate if node cell $C_i \in \mathcal{C}$ is energized at $t \in \mathcal{P}$ or $t \in \mathcal{T}$.
$s^N_{n,t}$	Binary to indicate if node $n \in \mathcal{N}$ is energized at $t \in \mathcal{P}$ or $t \in \mathcal{T}$.
$\boldsymbol{U}_{n,t} \in \mathbb{R}^{3\times1}$	Squared three-phase voltage magnitude of node $n \in \mathcal{N}$ at $t \in \mathcal{P}$ or $t \in \mathcal{T}$.
$\boldsymbol{P}^B_{ij,t} \in \mathbb{R}^{3\times1}$	Three-phase active power flowing through branch $(i,j) \in \mathcal{B}$ at $t \in \mathcal{P}$ or $t \in \mathcal{T}$.
$\boldsymbol{Q}^B_{ij,t} \in \mathbb{R}^{3\times1}$	Three-phase reactive power flowing through branch $(i,j) \in \mathcal{B}$ at $t \in \mathcal{P}$ or $t \in \mathcal{T}$.
$\boldsymbol{P}^L_{l,t} \in \mathbb{R}^{3\times1}$	Three-phase active load demand of load $l \in \mathcal{L}$ at $t \in \mathcal{P}$ or $t \in \mathcal{T}$.
$\boldsymbol{Q}^L_{l,t} \in \mathbb{R}^{3\times1}$	Three-phase reactive load demand of load $l \in \mathcal{L}$ at $t \in \mathcal{P}$ or $t \in \mathcal{T}$.

I. INTRODUCTION

LARGE-SCALE blackouts and extreme weather events in recent decades bring up the concern for developing resilient power infrastructures. Although many efforts have been made by researchers, utilities, and manufactures toward improving power system resilience and reliability, power outages cannot be completely prevented [1]. In face of destructive storms and coordinated cyber-physical attacks, even robustly operated power systems (e.g., based on "N-1" or "N-2" criteria) can be prone to cascading failures [2]. Unfortunately, power outages caused by extreme weather events have increased in the United States over the past decades [2]. For example, recent hurricanes Harvey, Irma, and Maria in 2017 caused massive damages to utilities' assets and extensive power outages [3]. Loss of electricity services further delayed critical rescue actions and affected the restoration processes of other dependent lifeline infrastructures such as communication, water, and gas systems [4]. Therefore, an efficient service restoration scheme is desired to restore electricity to customers as soon as possible after an outage.

Distribution networks contribute over 90% of the customer–outage minutes in the United States [5]. Power outages in distribution systems can be caused by unscheduled events (e.g., fallen trees, lightning, storms, and equipment failures) and scheduled events (e.g., regular maintenance and equipment installation). After outages have been detected and isolated, the distribution service restoration (DSR) will be performed to restore the out-of-service loads as soon as possible [6]. Traditionally, the DSR is performed by transferring the affected loads from out-of-service areas to healthy areas through a series of switching operations using alternative energization paths and operational criteria [7]. Nowadays, distribution systems are evolving toward active distribution systems (ADS) by incorporating increasing penetration of controllable devices that can actively regulate voltage and frequency, such as distributed generators (DGs) [8, 9], microgrids [10, 11], and remotely controllable switches [12, 13]. In the context of ADS, an advanced DSR framework is desired to generate optimal restoration solutions that can coordinate various controllable components to achieve optimal restoration performance. A feasible DSR solution should contain a sequence of temporally interdependent control actions that can be sequentially executed by operators and crews to control the field devices such as DGs, switches, and regulators [14]. However, most existing work focused mainly on generating a "snapshot" solution that represents the system configuration at a single instance in time. In some recent work, the restoration problems are formulated as dynamic optimization problems that consider the inter-temporal control and operational constraints of DGs and switches over a predetermined time horizon that is equally divided into multiple time steps [15-19]. In this paper, we categorize the dynamic optimization models using fixed time steps as fixed time step (FTS) models. FTS models assume that the switches are operated within the selected time interval (e.g., 1 hour). However, in distribution systems, both remotely controllable and manually operated switches are strategically installed, and the operating time for different types of switches can be significantly different. For example, operating a remotely controllable switch only needs a few minutes, whereas operating a manually operated switch will take much longer since restoration crews have to travel to the field and find the actual switch location. Existing FTS models cannot guarantee that the operation of manually operated switches will be finished within small time intervals, whereas using large time intervals will result in inefficient solutions. Therefore, the restoration solutions generated by the existing FTS models may not be readily applicable to distribution systems with heterogeneous types of switches.

Motivated by the aforementioned challenges, in this paper we propose an integrated DSR modeling framework including two DSR models: the FTS model and the variable time step (VTS) model. The FTS model, which is improved based on the authors' previous work [18, 19], can handle arbitrary operation time for automatic and manual switches. The VTS model is formulated based on the concept of a "virtual energization agent" and the vehicle routing model. The DSR modeling framework has the following modeling capabilities in addition to those found in the traditional restoration model: it (1) supports dispatchable DGs, (2) supports microgrid formation, (3) supports three-phase unbalanced power flow, (4) supports voltage regulator operation, (5) supports generating switching sequence, and (6) supports automatic and manual switch operation. All the above issues are practical considerations in the real-world power systems. To the best of our knowledge, this is the first time the VTS model is proposed to address the DSR problem while supporting all the above six modeling capabilities.

The main contributions of this paper are to:

(1) Propose an updated FTS DSR model that can handle different operating time of switches and other intertemporal constraints.
(2) Propose a novel VTS DSR model that can generate a restoration sequence and estimated time of restoration. The VTS model shows significant superiority in reducing computational complexity compared to the FTS model.
(3) Formulate both models as mixed-integer linear

programming (MILP) models, which can be readily solved by off-the-shelf solvers.

(4) Discuss and compare the proposed VTS and FTS models, as well as summarize their potential applications.

The remainder of this paper is organized as follows. Section II introduces the DSR modeling framework. Sections III and IV introduce the MILP formulation of the VTS and FTS models, respectively. Section V provides numerical results. Section VI discusses uncertainty and error issues and compares both models. Section VII summarizes the core findings and conclusions.

II. DSR Modeling Framework

A. Background

In traditional distribution systems, switches (e.g., substation breakers, sectionalizers, and tie-switches) are the only controllable devices used for developing alternative energization paths to bridge the power sources and the affected customers (i.e., reconfiguration). System operators rely on experience and computer programs to determine the energization paths and operation sequence of these switches. In this sense, the DSR problem is usually formulated as a combinatorial optimization problem with the energization status of switches as the decision variables. The combinatorial nature of the DSR problem makes it NP-complete and difficult to solve [20]. Therefore, some rule-based methods based on expert knowledge and heuristic and meta-heuristic methods (e.g., tabu search [20], fuzzy logic [21], expert system [22], and genetic algorithms [15]) are normally used to solve the DSR problem. However, these methods cannot guarantee the global optimality of the solutions [23]. On the other hand, mathematical optimization can potentially achieve global optimality. Some mathematical optimization models have been proposed for solving the traditional DSR problem [24, 25].

In the context of ADS, a wide variety of controllable components play active roles in the restoration process [18]. The increasing complexity of operating the modern distribution systems requires the restoration model to be able to incorporate the control policies of various controllable components, such as DGs, energy storage devices, voltage regulators, capacitor banks, and remote switches. TABLE I summarizes different types of controllable components in ADS.

TABLE I. Classification of Controllable Components in ADS

Type	Black Start Capability	Dispatch Capability	Examples
Black start DG	yes	yes	Diesel generator, gas turbine, steam turbine generator, micro turbine, fuel cell
Non-black start DG	no	yes	Micro turbine, small-hydro
		no	Wind generators, photovoltaics
Energy storage	yes, when discharging	yes	Battery, plug-in electric vehicle (PHEV), flywheel
Controllable loads	no	yes	Emergency demand response (DR) load (direct load control), economic DR load

In a DSR modeling framework, all the considered controllable components should be strategically modeled. In this situation, a modeling framework that can meet the modeling needs and can be conveniently adapted by the users is necessary to be developed. The models should achieve optimality guaranteed restoration solution within short time. Thus, we propose an integrated mixed-integer linear programming (MILP) model framework including two flexible models, fixed time step (FTS) model and variable time step model (VTS), which can adapt to the challenges mentioned above.

B. DSR Problem Formulation

The decision variables and state variables, as well as parameters of the DSR formulation are summarized in the Nomenclature. The node cells, same as the concept of node block introduced in [19], is defined as a set of nodes that are directly interconnected by non-switchable lines without being sectionalized by switches, thus all the lines within a cell will be energized at the same time. By defining node cells, the system topology can be reduced to a simpler topology with only node cells and switchable lines.

In this work, the objective function of the DSR problem is to minimize the total unserved energy over the considered horizon. As shown in Fig. 1, the time horizon is divided into multiple steps, and all loads are assumed to be energized by time step t_n. At each step, the total restored load can be formulated as the sum of all the energized loads. Then, the total unserved energy can be represented by the shaded area.

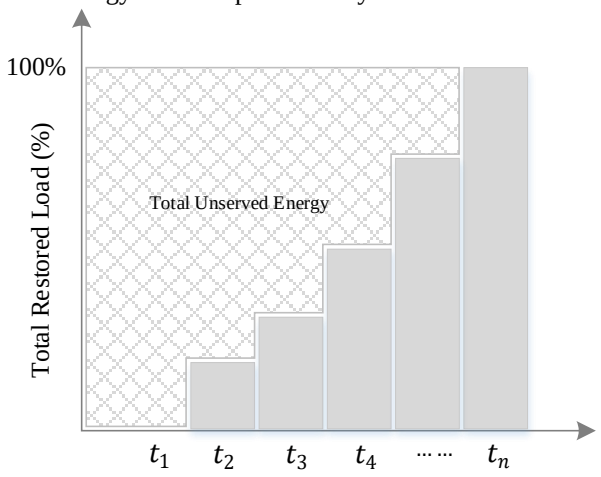

Fig. 1. Definition of the objective function of the DSR problem

Various constraints of the DSR formulations should be considered in DSR problems to ensure the feasibility of solutions. As shown in TABLE II, normally considered constraints can be divided into several categories: system model constraints, system operational constraints, component operation constraints, and topological constraints. In this paper, we assume that the energized system is always operated in radial topology. This is because although most distribution systems are constructed in meshed topology, they are normally operated in radial topology for protection, safety, and cost purposes. Different constraints can be added to address different concerns. For example, cold load pick-up (CLPU) issues and ZIP load models can be considered by revising the load model under the category of "system model constraints" [18, 19]. Transient stability and frequency issues, although not listed here, can be also considered as a set of constraints [26].

TABLE II. CONSTRAINTS IN THE DSR PROBLEM

Category	Constraints	Description
System Model Constraints	Power Flow	Model power flow equations
	Load	Model load demand
	Voltage Regulator	Model equivalent transformer
	DG and ESS	Model power output and input
	Initial Condition	Model initial state of the system
System Operational Constraints	Line Loading Capacity	Ensure the power going through each energized line is maintained below the thermal threshold
	Voltage Limit	Ensure the voltage magnitude of each energized bus is maintained within a permissive range
Component Operational Constraints	ESS Operation	Ensure each ESS is operated properly
	DG Operation	Ensure each DG is operated properly
	Regulator Operation	Ensure each regulator is operated properly
	Capacitor Operation	Ensure each capacitor is operated properly
Topological Constraints	Operating Time	Ensure switch is operated on time
	Connectivity and Sequencing	Ensure the sequence is feasibly generated, and energized feeders are in radial topology

III. VARIABLE TIME-STEP MODEL

In this section, a novel VTS model, which adopts the idea of the routing used for transportation sectors, is introduced to address the concern of the different operating time of switches over a long horizon.

A. MILP Formulation

1) The Concept of Virtual Energization Agent

We introduce the concept of "virtual energization agent" to help present the proposed VTS model. A virtual energization agent can "travel" along energization paths. The "travel time" for a virtual energization agent to travel from one node cell to another can be represented by the operating time of switches. In addition, different from conventional routing models, which require that an agent can only travel along a single route, a virtual energization agent can "split" into multiple agents and travel along multiple separate paths. A VTS model solution can be mapped to the DSR solution, as shown in Fig. 2. In the upper figure, Agent 1 travels along Path 1 (i.e., 1-2), then splits at node cell 2 and travels along two separate paths: Path 1 (1-2-3) and Path 2 (1-2-4). The lower figure shows that the actual system can be energized according to the energization paths (i.e., Path 1 and 2) while compliant with the operating time constraints.

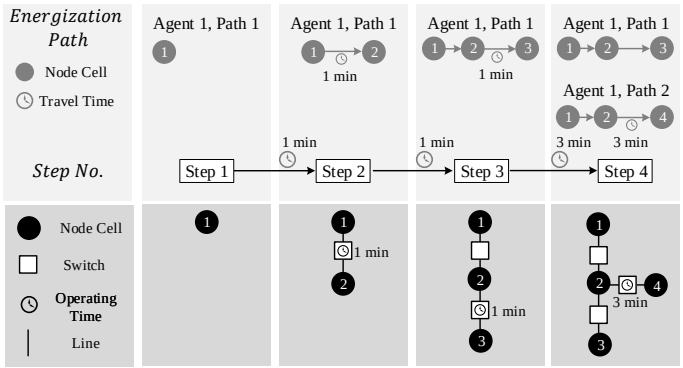

Fig. 2. An example of mapping the VTS model to the DSR solution. Agent 1 travels along Path 1 starting from node cell 1, then splits at node cell 2 and travels along two separate paths: 1-2-3 and 1-2-4.

2) Route Table to Represent Energization Paths

We introduce a route table to represent all the energization paths designated to all the virtual agents. Essentially, the route table can be modeled as the node incidence matrix of a directed graph. The route table is a $n^C \times n^C$ binary matrix ($n^C = |\mathcal{C}|$), of which each element x_{ij}^R indicates if there is a virtual energization agent travels from C_i to C_j. If an agent goes from C_i to C_j, $x_{ij}^R = 1$. Otherwise, $x_{ij}^R = 0$. Diagonal term $x_{ii}^R = 1$ if C_i contains a substation or a black start DG. Otherwise, $x_{ii}^R = 0$. If C_i and C_j are not connected through a switch, then $x_{ij}^R = 0$.

An example of a route table containing two energization paths is shown in Fig. 3. Node cell 1 contains a substation, which is the starting point for the virtual energization agents. Subfigure (b) shows the decision variables to be solved. Once the variables are solved, energization paths can be derived, as shown in subfigure (c). Each path starts with the diagonal term being "1" and travels along off-diagonal terms being "1".

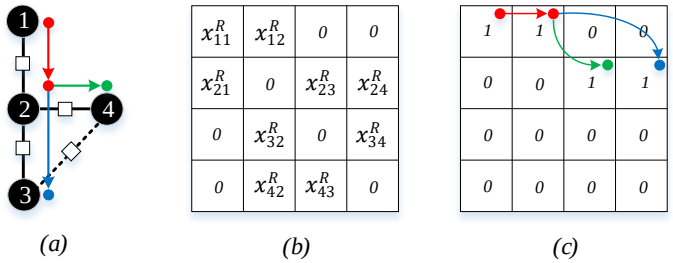

Fig. 3. An example of route table containing two energization paths (1-2-3 and 1-2-4): (a) energization paths, (b) variables defined in route table, and (c) values of variables representing energization paths.

3) Routing Model

In this paper, we focus on radially operated distribution systems. The routing model is described below and ensures the radial topology during the restoration process:

1) An energization path should start from a substation node or a black start DG:

$$x_{ii}^R = \begin{cases} 1, C_i \cap G^S \neq \emptyset \\ 0, C_i \cap G^S = \emptyset \end{cases} \quad (1)$$

2) An energization path should not go back to or go through a node cell containing a substation or a black start DG, to avoid forming a loop:

$$x_{ij}^R = 0, i \neq j, C_i \cap G^S = \emptyset, C_j \cap G^S \neq \emptyset. \quad (2)$$

3) An energization path should not contain a loop. In other words, a node cell in an energization path cannot be visited more than once:

$$x_{ij}^R + x_{ji}^R \leq 1, \ i \neq j. \quad (3)$$

4) A node cell can only be visited by at most one energization path:

$$\sum_i^{n^C} x_{ij}^R \leq 1. \quad (4)$$

5) Downstream node cells (e.g., C_k) of a node cell (e.g., C_j) can only be energized when the upstream node cell (e.g., C_i) is energized:

$$\sum_k^{n^C} x_{jk}^R \leq n^C \cdot \sum_i^{n^C} x_{ij}^R. \quad (5)$$

6) If two node cells cannot be connected by a switch, then there is no such route for an energization agent to travel through. Therefore, elements that represent "non-exist" routes in the route table should be zero:

$$x_{ij}^R = 0, (k,l) \notin \mathcal{B}^S, k,l \in C_i \cup C_j. \quad (6)$$

4) Restoration Time

From the traveling perspective, an energization agent always spends some time to travel from one node to another. The traveling time can be used for representing the operating time of the switch between the two nodes. Thus, we define a traveling time table to specify the operating time of each switch between two nodes, and an arrival time vector to represent the time when a node is energized. The following constraints can be used for calculating the arrival time when an energization agent arrives at node cell C_i.

$$T_{ii}^R - M(1 - x_{ii}^R) \le t_i \le T_{ii}^R + M(1 - x_{ii}^R), C_i \cap G^S \ne \emptyset \quad (7)$$

$$T^{Rmax} - M\sum_j^{n^C} x_{ji}^R \le t_i \le T^{Rmax} + M\sum_j^{n^C} x_{ji}^R \quad (8)$$

$$t_i + T_{ij}^R - M\left(1 - x_{ij}^R\right) \le t_j \le t_i + T_{ij}^R + M\left(1 - x_{ij}^R\right) \quad (9)$$

The big-M method is used to formulate the conditional constraint (7 – 9). Constraint (7) means that if and only if C_i contains a substation node or a black start DG (i.e., $x_{ii}^R = 1$), C_i will be energized at $t_i = T_{ii}^R$, otherwise t_i will not be constrained by (7). Constraint (8) implies that only if C_i is not visited by any energization agents (i.e., $\sum_j^{n^C} x_{ji}^R = 0$), t_i will be set to T^{Rmax}(where T^{Rmax} is the maximum restoration time), otherwise t_i will not be constrained by (8). Constraint (9) enforces $t_j = t_i + T_{ij}^R$ if and only if there is an agent travelling from C_i to C_j (i.e., $x_{ij}^R = 1$), otherwise t_i will not be constrained by (9). In this paper we choose the value of M to be T^{Rmax} for conditional constraints (7-9). The value of parameter T^{Rmax} is estimated based on the estimated time for dispatching crews, as well as performing repairs and restoration. In this paper, we take 1440 minutes (i.e., 1 day) as the value of T^{Rmax} in the case study part.

5) Check Point and Energization Status of Components

In the VTS model, we use the concept of "check point" instead of "time step" used in the FTS model. A check point is a time instance when we want to check operational constraints. Selection of a check point is "event-based". As explained later, we add an additional check point t_i before restoring C_i if C_i contains DGs with large capacity, and we add an additional check point t_p when no more node cells are energized. To distinguish them from the set of time steps $\mathcal{T}$, the set of check points is denoted as $\mathcal{P} \coloneqq \{t_1, t_2, \dots, t_i, \dots t_p\}$. The principles of choosing check points for VTS model is introduced in III.B. It is worth noting that the check points in $\mathcal{P}$ are not chronologically ordered.

The energization status of a component at a check point depends on whether this node cell is energized before/after this check point. Given a check point at time t_j (e.g., the time before energizing C_j or an arbitrarily selected time), the energization status of $C_i, i \ne j$ at time t_j (denoted as s_{C_i,t_j}^C) can be formulated as:

$$s_{C_i,t_j}^C = \begin{cases} 0, & t_i > t_j \\ 1, & t_i \le t_j \end{cases} \quad (10)$$

Similarly, the energization status of switchable line (k,l) at time t_j (denoted as x_{kl,t_j}^B) depends on whether or not this line is visited by an agent and if the node cells on both ends (denoted as C_m and C_n) are energized by t_j:

$$x_{kl,t_j}^B = (x_{mn}^R + x_{nm}^R) \wedge s_{C_m,t_j}^C \wedge s_{C_n,t_j}^C, \quad (k,l) \in \mathcal{B}^S, k,l \in C_m \cup C_n. \quad (11)$$

where $\wedge$ represents the logical term AND. For each interested check point, a set of constraints is defined to linearize Equations (10) and (11):

$$s_{C_i,t_i}^C = 0, \ t_i \in \mathcal{P}, i \ne p, \quad (12)$$

$$\frac{(t_j - t_i)}{M} \le s_{C_i,t_j}^C \le \frac{(t_j - t_i)}{M} + 1, \ t_i, t_j \in \mathcal{P}, i \ne j, j \ne p, \quad (13)$$

$$s_{C_i,t_p}^C = \sum_j^{n^C} x_{ij}^R, \ t_p \in \mathcal{P}, \quad (14)$$

$$a_{kl,t_j}^B \ge s_{C_m,t_j}^C + s_{C_n,t_j}^C - 1,$$
$$a_{kl,t_j}^B \le s_{C_m,t_j}^C, a_{kl,t_j}^B \le s_{C_n,t_j}^C,$$
$$x_{kl,t_j}^B \ge a_{kl,t_j}^B + (x_{mn}^R + x_{nm}^R) - 1,$$
$$x_{kl,t_j}^B \le a_{kl,t_j}^B, x_{kl,t_j}^B \le x_{mn}^R + x_{nm}^R,$$
$$(k,l) \in \mathcal{B}^S, k,l \in C_m \cup C_n, t_j \in \mathcal{P} \quad (15)$$

where $a_{kl,t_j}^B \in \{0,1\}$ is an auxiliary variable. Constraint (12) requires that the check point t_i^R is the time right before picking up C_i. Equation (10) is linearized by (13). Constraint (14) calculates the status at t_p. Note that because of constraint (3), $(x_{mn}^R + x_{nm}^R)$ is also a binary variable, thus by applying the equivalent linearization of logic AND or the product of two binary variables [27] twice, equation (11) is linearized into constraint (15). The energization status of other components can be guaranteed by the following:

$$s_{C_i,t}^C = s_{n,t}^N, C_i \subseteq \mathcal{C}, n \in C_i, t \in \mathcal{P}, \quad (16)$$

$$x_{ij,t}^B = s_{i,t}^N, x_{ij,t}^B = s_{j,t}^N, (i,j) \in \mathcal{B}\backslash(\mathcal{B}^S \cup \mathcal{B}^F), t \in \mathcal{P}, \quad (17)$$

$$x_{l,t}^L = s_{l,t}^N, \ l \in \mathcal{L}\backslash(\mathcal{L}^S \cup \mathcal{L}^F), t \in \mathcal{P}, \quad (18)$$

$$s_{g,t}^N = x_{g,t}^G, \quad g \in \mathcal{G}^S\backslash\mathcal{G}^F, t \in \mathcal{P}, \quad (19)$$

$$x_{g,t}^G \le s_{g,t}^N, \quad g \in \mathcal{G}\backslash(\mathcal{G}^S \cup \mathcal{G}^F), t \in \mathcal{P}, \quad (20)$$

$$x_{l,t}^L \le s_{l,t}^N, \ l \in \mathcal{L}^S\backslash\mathcal{L}^F, t \in \mathcal{P}, \quad (21)$$

$$x_{ij,t}^B \le s_{i,t}^N, x_{ij,t}^B \le s_{j,t}^N, (i,j) \in \mathcal{B}^S\backslash\mathcal{B}^F, t \in \mathcal{P}. \quad (22)$$

Constraint (16) ensures that the energization status of a node cell equals the status of each node within this node cell. Constraints (17) and (18) require that non-switchable lines and loads will be energized immediately when their terminal nodes are energized. Constraint (19) ensures a node is energized by a substation or black start DG. Constraints (20)-(22) require that a switchable DG, load, and line can only connect to the grid when their terminal nodes are energized. We assume all DGs are switchable.

Next, we introduce some commonly considered constraints listed in TABLE II. For simplicity, some models such as ESS are not presented but can be found in [18].

6) System Model Constraints

These are as follows:

$$\boldsymbol{U}_{i,t} - \boldsymbol{U}_{j,t} \le \widetilde{\boldsymbol{z}}_{ij}\boldsymbol{S}_{ij,t}^* + \widetilde{\boldsymbol{z}}_{ij}^*\boldsymbol{S}_{ij,t} + M\left(1 - x_{ij,t}^B\right)\boldsymbol{e}_{\boldsymbol{ij}}^{\boldsymbol{\phi}}, \quad (i,j) \in \mathcal{B}\backslash\mathcal{V}, t \in \mathcal{P}, \quad (23)$$

$$\boldsymbol{U}_{i,t} - \boldsymbol{U}_{j,t} \ge \widetilde{\boldsymbol{z}}_{ij}\boldsymbol{S}_{ij,t}^* + \widetilde{\boldsymbol{z}}_{ij}^*\boldsymbol{S}_{ij,t} - M\left(1 - x_{ij,t}^B\right)\boldsymbol{e}_{\boldsymbol{ij}}^{\boldsymbol{\phi}}, \quad (i,j) \in \mathcal{B}\backslash\mathcal{V}, t \in \mathcal{P}, \quad (24)$$

$$-M\left(1 - x_{ij,t}^B\right)\boldsymbol{e}_{\boldsymbol{ij}}^{\boldsymbol{\phi}} \le \boldsymbol{U}_{j,t} - \left(\boldsymbol{\beta}_{ij,t} + 1.01\boldsymbol{U}_{i,t} - 1.01\right) \le M\left(1 - x_{ij,t}^B\right)\boldsymbol{e}_{\boldsymbol{ij}}^{\boldsymbol{\phi}}, \ (i,j) \in \mathcal{V}, t \in \mathcal{P}, \quad (25)$$

$$\sum_{h:(h,i)\in B}\boldsymbol{P}_{hi,t}^B + \sum_{g:g=i,g\in\mathcal{G}}\boldsymbol{P}_{g,t}^G = \sum_{j:(i,j)\in B}\boldsymbol{P}_{ij,t}^B + \sum_{l:l=i,l\in\mathcal{L}}\boldsymbol{P}_{l,t}^L, (i,j) \in \mathcal{B}, t \in \mathcal{P}, \quad (26)$$

$$\sum_{h:(h,i)\in B}\boldsymbol{Q}_{hi,t}^B + \sum_{g:g=i,g\in\mathcal{G}}\boldsymbol{Q}_{g,t}^G = \sum_{j:(i,j)\in B}\boldsymbol{Q}_{ij,t}^B +$$

$$\sum_{l:l=i,l\in\mathcal{L}} \boldsymbol{Q}^L_{l,t}, (i,j)\in\mathcal{B}, t\in\mathcal{P}, \quad (27)$$

$$\boldsymbol{P}^G_{g,t} \le x^G_{g,t}\cdot \boldsymbol{P}^{max}_g,\ \boldsymbol{Q}^G_{g,t} \le x^G_{g,t}\cdot \boldsymbol{Q}^{max}_g, g\in\mathcal{G}, t\in\mathcal{P}, \quad (28)$$

$$\boldsymbol{P}^L_{l,t} = x^L_{l,t}\cdot \boldsymbol{P}^{LN}_l,\ \boldsymbol{Q}^L_{l,t} = x^L_{l,t}\cdot \boldsymbol{Q}^{LN}_l, l\in\mathcal{L}, t\in\mathcal{P}, \quad (29)$$

$$x^G_{g,t}=1, \boldsymbol{U}_{g,t}=[1.0,1.0,1.0]^T, g\in\mathcal{G}^S\backslash\mathcal{G}^F, t\in\mathcal{P}, \quad (30)$$

$$x^B_{ij,t}=0,\ (i,j)\in\mathcal{B}^S\backslash\mathcal{B}^F, t=1, \quad (31)$$

$$x^B_{ij,t}=0, x^G_{g,t}=0, s^N_{n,t}=0, x^L_{l,t}=0,$$
$$(i,j)\in\mathcal{B}^F, g\in\mathcal{G}^F, n\in\mathcal{N}^F, l\in\mathcal{L}^F, t\in\mathcal{P}, \quad (32)$$

where $\tilde{\boldsymbol{z}}_{ij}\in\mathbb{C}^{3\times3}$ is the equivalent line impedance matrix consisting of constant values defined in [19], $\boldsymbol{S}_{ij,t}=\boldsymbol{P}^B_{ij,t}+j\boldsymbol{Q}^B_{ij,t}$, and $\boldsymbol{e}^{\phi}_{ij}\in\{0,1\}^{3\times1}$ is a vector with binary entries to represent phases. Constraints (23)-(27) are power flow constraints describing the voltage difference between two end nodes of each line and the voltage regulator, as well as the power balance at each node. Constraints (28) and (29) require DG outputs and load demands to be zero when de-energized. Constraints (30)-(32) specify initial conditions. Rather than using three-phase balanced power flow formulations in linearized restoration models [25, 28, 29], three-phase unbalanced power flow formulations are applied in the proposed framework because the real distribution system is naturally three-phase unbalanced [30]. First, constraints (23) – (24) formulate the linearized three-phase line model as introduced in [19]. Moreover, the three-phase voltage regulator can be modeled as a non-linear term $\boldsymbol{U}_{j,t}=\boldsymbol{\beta}_{ij,t}\odot\boldsymbol{U}_{i,t}$, which can be further linearized as constraint (25). Based on the fact that the per unit values [31] of $\boldsymbol{\beta}_{ij,t}$ and $\boldsymbol{U}_{i,t}$ change within narrow ranges ($\boldsymbol{\beta}_{ij,t}\in[0.9^2,1.1^2]$ because of a $\pm$ 10% regulator range [36], and $\boldsymbol{U}_{i,t}\in[0.95^2,1.05^2]$ because of a $\pm$ 5% service voltage range [32]), so the bilinear term $\boldsymbol{\beta}_{ij,t}\odot\boldsymbol{U}_{i,t}$ (the operator $\odot$ denotes element-wise product) can be approximated by a linear function:

$$\boldsymbol{\beta}_{ij,t}\odot\boldsymbol{U}_{i,t} \approx \boldsymbol{a}\odot\boldsymbol{\beta}_{ij,t}+\boldsymbol{b}\odot\boldsymbol{U}_{i,t}+\boldsymbol{c} \quad (33)$$

where $\boldsymbol{a}$, $\boldsymbol{b}$, and $\boldsymbol{c}\in\mathbb{R}^{3\times1}$ are denoted as the coefficients for the linear model, and they can be determined by solving the following quadratic programming problem:

$$\min \left\| \left(\boldsymbol{\beta}_{ij,t}\odot\boldsymbol{U}_{i,t}\right) - \left(\boldsymbol{a}\odot\boldsymbol{\beta}_{ij,t}+\boldsymbol{b}\odot\boldsymbol{U}_{i,t}+\boldsymbol{c}\right) \right\| \quad (34)$$

$$s.t.\ 0.9^2 \le \boldsymbol{\beta}_{ij,t} \le 1.1^2 \quad (35)$$

$$0.95^2 \le \boldsymbol{U}_{i,t} \le 1.05^2 \quad (36)$$

Note we only need to solve the problem (34)-(36) once. By solving the above model, the optimal approximation parameters are obtained: $\boldsymbol{a}=[1,1,1]^T$, $\boldsymbol{b}=[1.01,1.01,1.01]^T$, and $\boldsymbol{c}=[-1.01,-1.01,-1.01]^T$. The error introduced by modeling the ratios determined by discrete tap positions as continuous variables can be neglected [33].

7) System Operational Constraints

These are as follows:

$$-\boldsymbol{P}^{max}_{ij}\cdot x^B_{ij,t} \le \boldsymbol{P}^B_{ij,t} \le \boldsymbol{P}^{max}_{ij}\cdot x^B_{ij,t}, (i,j)\in\mathcal{B}, t\in\mathcal{P} \quad (37)$$

$$-\boldsymbol{Q}^{max}_{ij}\cdot x^B_{ij,t} \le \boldsymbol{Q}^B_{ij,t} \le \boldsymbol{Q}^{max}_{ij}\cdot x^B_{ij,t}, (i,j)\in\mathcal{B}, t\in\mathcal{P}, \quad (38)$$

$$s^N_{i,t}\cdot\boldsymbol{U}^{min} \le \boldsymbol{U}_{i,t} \le s^N_{i,t}\cdot\boldsymbol{U}^{max},\ \ i\in\mathcal{N}, t\in\mathcal{P}, \quad (39)$$

Constraints (37)-(39) require line loading conditions, and nodal voltages should be maintained within safe margins.

8) Component Operational Constraints

These are as follows:

$$P^{min}_g \le \sum_{\phi\in\{a,b,c\}} P^{\phi}_{g,t} \le x^G_{g,t}\cdot P^{max}_g, g\in\mathcal{G}, t\in\mathcal{P} \quad (40)$$

$$Q^{min}_g \le \sum_{\phi\in\{a,b,c\}} Q^{\phi}_{g,t} \le x^G_{g,t}\cdot Q^{max}_g, g\in\mathcal{G}, t\in\mathcal{P} \quad (41)$$

$$\boldsymbol{\beta}^{min}_{ij} \le \boldsymbol{\beta}_{ij,t} \le \boldsymbol{\beta}^{max}_{ij}, (i,j)\in\mathcal{V}, t\in\mathcal{P} \quad (42)$$

In this paper, we assume all the DGs are three-phase. Constraints (40)-(42) guarantee safe operation of DGs and voltage regulators.

9) Objective Function

The objective is to minimize the unserved energy:

$$\min \sum_{l\in\mathcal{L}}\sum_{t\in\mathcal{P}}\sum_{\phi\in\{a,b,c\}} \omega^L_l\cdot P^{\phi}_l\cdot t^R_{k:l\in\mathcal{C}_k} \quad (43)$$

The constraints are given in (1)-(9), (12)-(32), and (37)-(42).

B. Voltage Drops and Line Loading in Radial Systems

In a radially operated distribution system, before large numbers of DGs are connected, the voltage profiles and line loading conditions are monotonically changed along feeders under the assumption that the system is three-phase balanced [30]. Thus, restoring an additional load at check point t will lower the entire voltage profile and increase the loading of upstream lines compared with the system configuration before the additional load is restored. If the voltage and line loading constraints are satisfied at the check point t, they must be satisfied for the time duration before t when only loads and lines are energized. In this paper, we assume that this also applies to three-phase unbalanced distribution systems. Indeed, energizing some single-phase loads may not guarantee the lowering of all three-phase voltages. One can avoid this situation by properly placing switches during the planning stage, and thus a nearly-balanced three-phase load can be achieved within each node cell.

By contrast, DGs of large capacity can cause reverse current, thus reshaping voltage profiles and line loading conditions. Therefore, voltage profiles and line loading conditions no longer monotonically change along the feeder. In this situation, additional check points should be added before energizing a node cell containing large DGs, as shown in Fig. 4. Voltage is monotonically decreasing along the feeder in conditions 1 and 2. In condition 3, energizing a large DG may increase the entire voltage profile a level, thus a check point before restoring the large DG should be added to check the voltage at condition 2. Even though the voltage regulator can step up the voltage of downstream nodes (e.g., condition 5), its upstream nodes will still experience decreasing voltage as more loads are restored (e.g., condition 6). Finally, a check point is added when no more loads are restored (i.e., condition 6), since the overall voltage profile is normally at the lowest level in this condition.

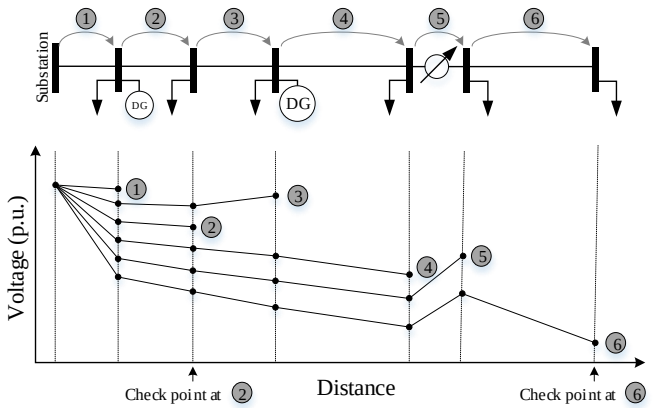

Fig. 4. An example of six voltage profiles corresponding to six conditions representing six sequential switching actions applied to a simple radial feeder.

IV. Fixed Time-Step Model

The FTS model is commonly used for incorporating intertemporal constraints, such as the DG ramping rate limit and time-changing load demand under CLPU conditions [18]. Considering the DSR problem over a time span from $t = 0$ (i.e., the beginning of restoration) to $t = T$ (i.e., the time when the last restorable load is energized), the time horizon can be denoted as $[0, T]$, and the time step set is denoted as $\mathcal{T} \coloneqq \{t_1, t_2, \dots t_n\}$ with $t_1 = 0$ and $t_n = T$ as the set of discrete time steps. As the model's name implies, the length of interval $\Delta t = t_{k+1} - t_k$ is fixed between any two consecutive steps. After decision variables at each time step are determined, the system operator can implement the control actions sequentially from t_0 to t_n. Figure 5 shows an example DSR solution with the FTS model. The time step is fixed to be 1 minute. The energization sequence can be derived based on the values of decision variables. The energized system diagram at each time step is also shown. Note that the operating time for the switch between Node 2 and Node 4 is 3 minutes, so it takes three steps (i.e., 3 minutes) to energize this switch. As a result, no control actions are performed at the 3rd minute due to the longer operating time of the switch.

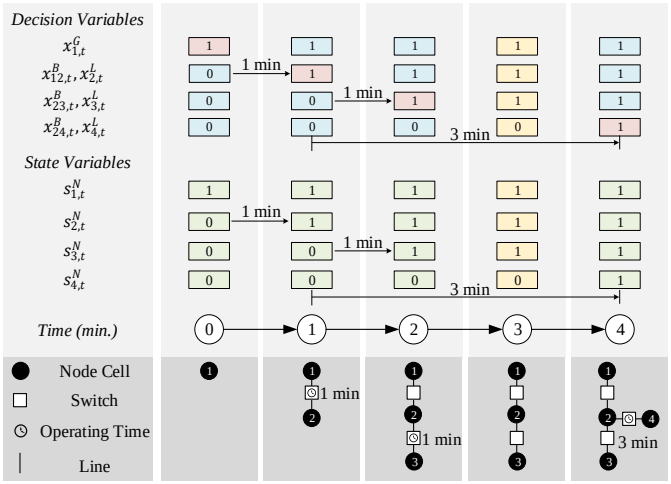

Fig. 5. An example of DSR solution of the FTS model. Only binary variables are shown. No control is performed at the 3rd minute due to the longer operating time of the switch between Node 2 and Node 4.

A. MILP Formulation

In the FTS model, system model constraints, system operational constraints, and component operational constraints can also be found in (23)-(32) and (37)-(42). In these constraints, the set of time steps is changed to $\mathcal{T}$, since these constraints are also applicable for the system configuration at each time step and independent of the chronological order. Next, the connectivity and sequencing constraints and operating time constraints are introduced.

1) Connectivity and Sequencing Constraints

These are as follows:

$$x^G_{g,t} \geq x^G_{g,t-1},\ g \in \mathcal{G}, t \in \mathcal{T}, t > 1, \quad (44)$$

$$x^L_{l,t} \geq x^L_{l,t-1},\ l \in \mathcal{L}^S, t \in \mathcal{T}, t > 1, \quad (45)$$

$$x^B_{ij,t} \geq x^B_{ij,t-1},\ (i,j) \in \mathcal{B}^S \backslash \mathcal{B}^F, t \in \mathcal{T}, t > 1, \quad (46)$$

$$\left(s^C_{C_m,t} - s^C_{C_m,t-1}\right) + \left(s^C_{C_k,t} - s^C_{C_k,t-1}\right) \geq x^B_{(i,j),t} - x^B_{(i,j),t-1},$$
$$(i,j) \in \mathcal{B}^S, i \in C_m, j \in C_k, t \in \mathcal{T}, t > 1, \quad (47)$$

$$\sum_{j:\,(i,j)\in\mathcal{B}^S}\left(x^B_{ij,t} - x^B_{ij,t-1}\right) + \sum_{k:\,(k,i)\in\mathcal{B}^S}\left(x^B_{ki,t} - x^B_{ki,t-1}\right) \leq 1 + Ms^C_{C_m,t-1},\ i \in C_m, t \in \mathcal{T}, t > 1, \quad (48)$$

$$s^C_{C_m,t} \leq \sum_{i:\,(i,j)\in\mathcal{B}^S} x^B_{ij,t} + \sum_{i:\,(k,i)\in\mathcal{B}^S} x^B_{ki,t},\ i \in C_m, t \in \mathcal{T}, \quad (49)$$

$$x^B_{(i,j),t} \leq s^C_{m,t-1} + s^C_{k,t-1},$$
$$(i,j) \in \mathcal{B}^S, i \in C_m, j \in C_k, t \in \mathcal{T}, t > 1. \quad (50)$$

Connectivity constraints are formulated and explained in (16)-(22). We assume all DGs are switchable. Constraints (44)-(46) require that a DG, load, or line should not be disconnected once being energized. Constraints (47)-(50) ensure the restoration sequence can be properly generated while the energized system is radially operated at each time step [19].

2) Operating Time Constraints

In the FTS model, the operating time of a switch $(i,j) \in \mathcal{B}^S$ can be denoted as $n^{op}_{ij} \cdot \Delta t$, with n^{op}_{ij} being the total number of steps needed for operating the switch. The total energization duration of Node i can be formulated as $\sum_{t\in\mathcal{T}} s^N_{i,t} \cdot \Delta t$. If Node i is energized at step k, then $\sum_{t=1}^{k-1} s^N_{i,t} \cdot \Delta t = 0$. Now, if closing a switch (i,j) to energize Node j, it will take at least $n^{op}_{ij} \cdot \Delta t$ amount of time to operate the switch. The actual operating time T_{ij} can be formulated as:

$$T_{ij} = \left(\sum_{t\in\mathcal{T}} s^N_{i,t} - \sum_{t\in\mathcal{T}} x^B_{ij,t}\right)\Delta t + \left(\sum_{t\in\mathcal{T}} s^N_{j,t} - \sum_{t\in\mathcal{T}} x^B_{ij,t}\right)\Delta t,$$
$$(i,j) \in \mathcal{B}^S \quad (51)$$

In (51), the first term of the right-hand side represents the duration between the step when Node i is energized and the step when switch (i,j) is closed. Since Node j will be energized immediately when switch (i,j) are closed, the second term equals zero. Similarly, (51) can be used for representing the operating time when closing switch (i,j) to energize Node i through Node j. Then, the operating time constraint can be formulated as:

$$T_{ij} \geq n^{op}_{ij} \cdot \Delta t - M\left(1 - x^B_{ij,t_n}\right), (i,j) \in \mathcal{B}^S. \quad (52)$$

3) Objective Function

Assume the objective is to minimize the unserved energy; then, the FTS model based on MILP formulation is:

$$\min \sum_{l\in\mathcal{L}} \sum_{t\in\mathcal{T}} \sum_{\phi\in\{a,b,c\}} \omega^L_l \cdot P^{\phi}_l \cdot \left(1 - x^L_{l,t}\right) \cdot \Delta t \quad (53)$$

The constraints are given in (16)-(32), (37)-(42) and (44)-(53).

V. Numerical Results

In this section, we validate and compare the proposed FTS and VTS MILP models, which are solved by CPLEX 12.6 on an Intel Core i7-6820HQ (with 2.7-GHz CPU, 16 GB of RAM, and 64-bit operating system), and the optimality gap is set to be the default value used in the CPLEX solver.

A. Test System and Case Design

We used the IEEE 123 node test feeder available in [34] to validate the proposed MILP models. The system contains multiple substations, unbalanced load conditions, voltage regulators, and capacitor banks. Additional switchable lines and DGs are added to the original test feeder, and the system is partitioned into 15 node cells, as shown in Fig. 6. In addition, the system is assumed to operate under heavy loading conditions by doubling the original loading demand. The DG parameters are listed in TABLE III. The operating times of switchable lines are listed in TABLE IV.

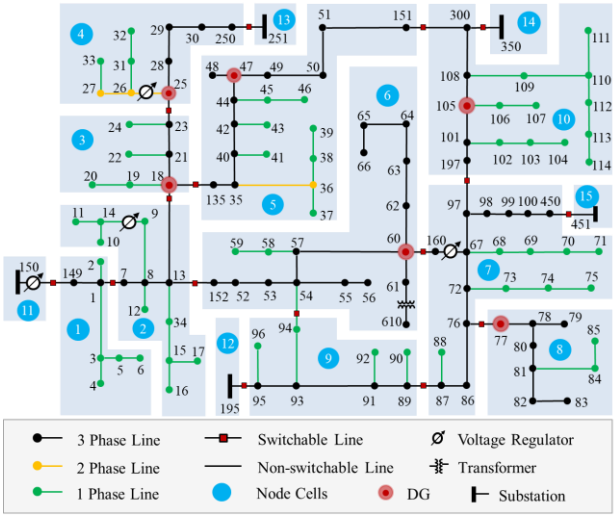

Fig. 6. Modified IEEE 123 node test feeder partitioned into 15 node cells by 16 switches.

TABLE III. DG PARAMETERS

Name	Node	P_g^{max}/P_g^{min} (kW)	Q_g^{max}/Q_g^{min} (kVar)
DG18	18	1000/100	800/-800
DG25	25	80/8	60/-60
DG47	47	100/10	50/-50
DG60	60	120/12	90/-90
DG77	77	800/80	300/-300
DG105	105	60/6	30/-30

TABLE IV. OPERATING TIME OF SWITCHABLE LINES

Line	Time (min)	Line	Time (min)
(1, 7)	8	(97, 197)	1
(13, 18)	10	(150, 149)	1
(23, 25)	12	(250, 251)	1
(76, 77)	14	(450, 451)	1
(87, 89)	16	(54, 94)	20
(13, 152)	1	(151, 300)	22
(18, 135)	18	(300, 350)	1
(60, 160)	1	(95, 195)	1

Three cases studies were designed to validate and compare the performance of the FTS and VTS models. In Case 1, five substations are available for DSR while all the dispatchable DGs are disabled. In Case 2, only the substation on Node 150 is available for DSR, and all the other substations and dispatchable DGs are assumed to be unavailable. In Case 3, the substation on Node 150 and all the dispatchable DGs are utilized as power source during DSR. For all three cases, the test system is assumed to be completely de-energized before DSR. The time step used in the FTS model is assumed to 1 minute.

B. Numerical Results

The total restored loads and energy, as well as the computation time for all cases are summarized in TABLE V. The data indicate that FTS and VTS models achieve the same objective values for all cases. However, the computation time used by the VTS model is almost 90% less than the FTS model.

TABLE V. RESTORED LOADS, ENERGY AND COMPUTATION TIME

	VTS Model			FTS Model		
Case	1	2	3	1	2	3
Restored Loads (kW)	6770	4930	6770	6770	4930	6770
Restored Energy (kWh)	1673	1638	1859	1673	1638	1859
Computation Time (s)	2.3	2.4	3.2	17.9	27.9	22.1

The switch-on sequence and cells energization sequence are listed in TABLE VI. Once a node cell is energized, all the loads inside the node cell are energized thus the estimated time of restoration for all the loads inside the node cell is known according to TABLE VI. Note the VTS mode and the FTS model have generated restoration solutions with identical energization sequences for all three cases. The total required restoration time is 23 minutes for Case 1, 37 minutes for Case 2, and 34 minutes for Case 3. Note the total required restoration time is derived from the VTS model. As for the FTS model, a pre-determined time horizon must be selected. Implied by the VTS solutions, the FTS time horizon is set to 23 minutes for Case 1, 37 minutes for Case 2, and 34 minutes for Case 3. These values are the shortest time horizons that ensure the FTS model can achieve the same objective value with the VTS model.

TABLE VI. DSR SWITCHING SEQUENCE FOR CASE 1, 2, AND 3*

Time (min)	Switch-on Sequence			Cells Energization		
	Case 1	Case 2	Case 3	Case 1	Case 2	Case 3
0	None	None	None	None	None	None
1	(150, 149)	(150, 149)	(150, 149)	1	1	1
	(250, 251)			4		
	(300, 350)			10		
	(450, 451)			7		
	(95, 195)			9		
9	(1, 7)	(1, 7)	(1, 7)	2	2	2
10	(13, 152)	(13, 152)	(13, 152)	6	6	6
11		(60, 160)	(60, 160)		7	7
12			(97, 197)			10
13	(23, 25)			3		
15	(76, 77)			8		
19		(13, 18)	(13, 18)		3	3
23	(151, 300)			5		
25			(76, 77)			8
27			(87, 89)			9
31			(23, 25)			4
34			(151, 300)			5
37		(18, 135)			5	

* VTS and FTS models have generated restoration solutions with identical energization sequences for Case 1, 2, and 3.

In Case 1, as shown in Fig. 7, the system is partitioned into 5 subsystems, each of which is energized by one substation. all loads are restored. As listed in TABLE VI, all the substation breakers are closed at the 1st minute. Then, the remotely controlled and manually operated switches are closed sequentially. All the loads are eventually restored within 23 minutes. In Case 2, the system is partially restored, and all the restored loads are powered by substation on Node 150. Some nodes cannot be restored due to the heavy loading conditions, which can lower the voltage profiles and overload lines. In Case 3, the system is totally restored, and all the restored loads are powered by substation on Node 150 and 6 dispatchable DGs. Dispatchable DGs are used for mitigating voltage and line loading conditions, and thus more loads are restored compared to that of Case 2.

For a more detailed illustration of the multi-step restoration process, the restored loads at each time step for Case 3 are shown in Fig.8. Blue bars represent check points considered in the VTS model. Grey bars plus blue bars represent the steps considered in the FTS model. It can be clearly seen that the size of the VTS model is much smaller than the FTS model, and thus, computation time can be effectively reduced.

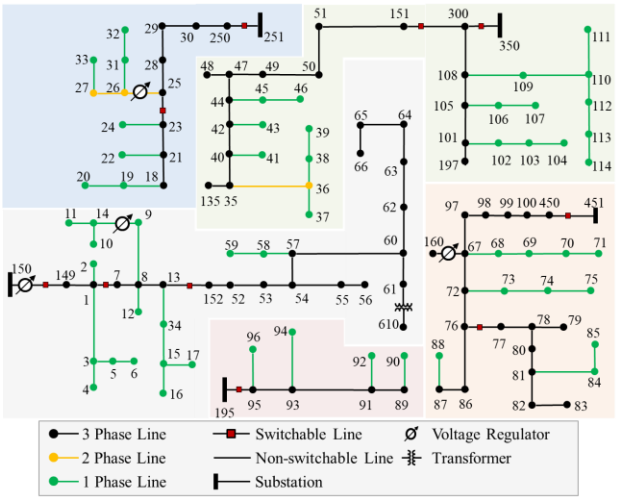

Fig. 7. Energized system in Case 1. The system is partitioned into 5 subsystems and all loads are restored.

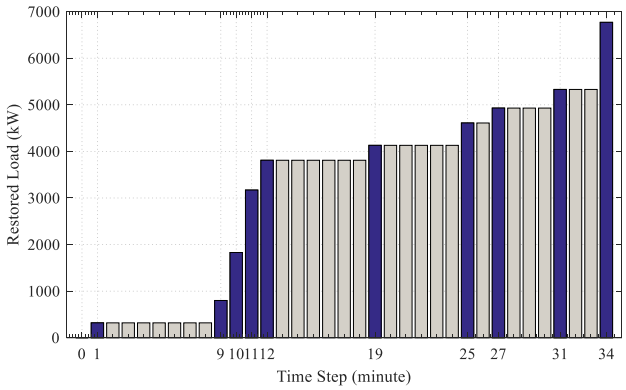

Fig. 8. Restored loads at each time step in Case 3. Blue bars for VTS model, while grey bars plus blue bars for FTS model.

VI. Discussion

A. Dealing with Uncertainties and Errors

First, it is worth mentioning that the restoration process is carried out in two stages: the planning stage and the execution stage, and the uncertainties and errors exist in both stages. In the planning stage, the DSR solutions are generated by solving the proposed models based on the information collected from DMS, OMS, SCADA, and the customer information system (CIS). Uncertainties and errors existing in this stage include: (1) load forecasting errors, (2) damage assessment errors, and (3) system parameter errors. The adverse effects of uncertainties might be mitigated by formulating the DSR problem as a stochastic programming problem [29] or a robust programming problem [8]. Both the FTS and VTS models can be incorporated into the formulation of stochastic and robust programming models, which will be considered in the future work.

Uncertainties and errors also exist in the execution stage of the restoration process, in which the system operator and crews will execute the predetermined restoration solution by energizing the physical components sequentially. To ensure that the restoration process is precisely controlled and that operation constraints (e.g., voltage magnitude and line thermal limit) are satisfied, the system state variables and topology need to be monitored continuously based on the measurements collected from the sensors and meters installed in the network. In this sense, any errors (e.g., meter biases, telecommunication failures, malfunction and unreported position status of switches) contained in the measurement data can result in biased state estimation, unobservable system states, and topology errors, and these errors can eventually mislead and delay the restoration process. In this regard, an effective error detection and identification approach, as well as a calibration and correction approach with good convergence properties, as reported in [35, 36], are desired to help ensure that the restoration scheme is accurately executed.

B. Comparison of FTS and VTS Models

Although serving the same objective, the proposed FTS and VTS models have both advantages and disadvantages with respect to the other. The VTS model allows the operation time of both remotely controlled and manually controlled switches to be easily considered based on the concept of a "virtual energization agent". Unlike in the FTS model, the switching sequence is formulated in the route table in the VTS model. In addition, the VTS model leverages voltage drops and line-loading characteristics in radial distribution systems based on the concept of a "check point." Thus, the operational constraints need only to be checked at limited check points even though the restoration is performed through many more switching actions. In this sense, the complexity of the problem formulation can be effectively reduced. However, the FTS model must define both decision and state variables at each time step, causing the problem size to grow quickly with the predetermined time steps. Moreover, without knowing the estimated time of restoration, the time horizon used for solving the FTS model is quite difficult to determine. A large time horizon may ensure optimality but requires a longer computation time; however, a smaller time horizon is time-saving but generates less optimal solutions. In practice, a restoration process usually takes a long time, which means that a very large number of time steps should be defined in the FTS model and result in an extended computational burden. However, the FTS model can easily incorporate inter-temporal operational constraints and control policies, such as power output profiles of renewable DGs, time-varying load demand and response, and the charging/discharging behaviors of ESS, whereas considering these constraints is difficult in the VTS model. In this regard, the motivation of this work is to introduce both models that can address restoration challenges under various scenarios.

VII. Conclusion

The core contribution of this work is to propose a DSR framework that can adapt to the complex operation environment of ADS. Controllable components and associated operational constraints were summarized. Two DSR modeling methods were introduced and compared, namely, the FTS model and the VTS model. Both models target at solving issues in real-world DSR problems with various practical considerations, such as (1) unbalanced loads, (2) three-line un-transposed lines, (3) voltage regulator control, (4) capacitor banks, (5) multiple switches with different operating times, and (6) some advanced capabilities in the context of smart

distribution systems (e.g., DG dispatch and microgrid formation). The VTS model was first proposed based on the concepts of "virtual energization agent" and "check point," which allow the operation time of both remotely controlled and manually controlled switches to be easily considered. The route table was used to formulate the switching sequence in the VTS model, thus effectively reducing the complexity of the problem formulation. Meanwhile, an FTS model was also proposed based on the authors' previous work by incorporating the different operating times of both remotely controlled and manually controlled switches. Case study results show that the VTS model achieved the same energization sequence solution as the FTS model with much less computation time. However, the inter-temporal operational constraints can be easily formulated in the FTS model while not in the VTS model. The advantages and disadvantages of both models were discussed. Also, we discussed the existence and possible mitigating methods of uncertainties and errors during the DSR. Future work includes the evaluation of the VTS model for solving large-scale, real-world power systems, and further modeling and decomposition techniques should also be developed accordingly.

REFERENCES

[1] National Academies of Sciences, Engineering and Medicine, *Enhancing the Resilience of the Nation's Electricity System*, Washington, DC: The National Academies Press, 2017.

[2] Y. Wang, C. Chen, J. Wang, and R. Baldick, "Research on Resilience of Power Systems Under Natural Disasters-A Review," *IEEE Transactions on Power Systems*, vol. 31, no. 2, pp. 1604-1613, 2016.

[3] US. Dept. of Energy, "Hurricanes Nate, Maria, Irma, and Harvey Situation Reports", Oct. 13, 2017. [Online]. Available: https://www.energy.gov/oe/downloads/hurricanes-nate-maria-irma-and-harvey-situation-reports.

[4] M. Panteli, and P. Mancarella, "Modeling and Evaluating the Resilience of Critical Electrical Power Infrastructure to Extreme Weather Events," *IEEE Systems Journal*, vol. 11, no. 3, pp. 1733-1742, 2017.

[5] R. J. Campbell, *Weather-Related Power Outages and Electric System Resiliency:* Congressional Research Service, Liabrary of Congress, 2012.

[6] A. Zidan, M. Khairalla, A. M. Abdrabou, T. Khalifa, K. Shaban, A. Abdrabou, R. E. Shatshat, and A. M. Gaouda, "Fault Detection, Isolation, and Service Restoration in Distribution Systems: State-of-the-Art and Future Trends," *IEEE Transactions on Smart Grid*, vol. 8, no. 5, pp. 2170-2185, 2017.

[7] J. Li, X. Y. Ma, C. C. Liu, and K. P. Schneider, "Distribution System Restoration With Microgrids Using Spanning Tree Search," *IEEE Transactions on Power Systems*, vol. 29, no. 6, pp. 3021-3029, 2014.

[8] X. Chen, W. Wu, and B. Zhang, "Robust Restoration Method for Active Distribution Networks," *IEEE Transactions on Power Systems*, vol. 31, no. 5, pp. 4005-4015, 2016.

[9] Q. Chen, X. Zhao, and D. Gan, "Active-reactive scheduling of active distribution system considering interactive load and battery storage," *Protection and Control of Modern Power Systems*, vol. 2, no. 1, pp. 29, 2017/08/07, 2017.

[10] J. Liu, H. Chen, W. Zhang, B. Yurkovich, and G. Rizzoni, "Energy Management Problems Under Uncertainties for Grid-Connected Microgrids: A Chance Constrained Programming Approach," *IEEE Transactions on Smart Grid*, vol. 8, no. 6, pp. 2585-2596, 2017.

[11] J. Liu, W. Zhang, and G. Rizzoni, "Robust Stability Analysis of DC Microgrids With Constant Power Loads," *IEEE Transactions on Power Systems*, vol. 33, no. 1, pp. 851-860, 2018.

[12] Y. Xu, C. C. Liu, K. P. Schneider, and D. T. Ton, "Placement of Remote-Controlled Switches to Enhance Distribution System Restoration Capability," *IEEE Transactions on Power Systems*, vol. 31, no. 2, pp. 1139-1150, 2016.

[13] S. Lei, J. Wang, and Y. Hou, "Remote-Controlled Switch Allocation Enabling Prompt Restoration of Distribution Systems," *IEEE Transactions on Power Systems*, vol. 33, no. 3, pp. 3129-3142, 2018.

[14] C. Chen, J. Wang, and D. Ton, "Modernizing Distribution System Restoration to Achieve Grid Resiliency Against Extreme Weather Events: An Integrated Solution," *Proceedings of the IEEE*, vol. 105, no. 7, pp. 1267-1288, 2017.

[15] I. Watanabe, and M. Nodu, "A genetic algorithm for optimizing switching sequence of service restoration in distribution systems." *Proceedings of the 2004 Congress on Evolutionary Computation*, 2004, pp. 1683-1690 Vol.2.

[16] R. Perez-Guerrero, G. T. Heydt, N. J. Jack, B. K. Keel, and A. R. Castelhano, "Optimal Restoration of Distribution Systems Using Dynamic Programming," *IEEE Transactions on Power Delivery*, vol. 23, no. 3, pp. 1589-1596, 2008.

[17] Z. Wang, and J. Wang, "Self-Healing Resilient Distribution Systems Based on Sectionalization Into Microgrids," *IEEE Transactions on Power Systems*, vol. 30, no. 6, pp. 3139-3149, 2015.

[18] B. Chen, C. Chen, J. Wang and K. L. Butler-Purry, "Multi-Time Step Service Restoration for Advanced Distribution Systems and Microgrids," in *IEEE Transactions on Smart Grid*, vol. 9, no. 6, pp. 6793-6805, Nov. 2018.

[19] B. Chen, C. Chen, J. Wang and K. L. Butler-Purry, "Sequential Service Restoration for Unbalanced Distribution Systems and Microgrids," in *IEEE Transactions on Power Systems*, vol. 33, no. 2, pp. 1507-1520, March 2018.

[20] S. Toune, H. Fudo, T. Genji, Y. Fukuyama, and Y. Nakanishi, "Comparative study of modern heuristic algorithms to service restoration in distribution systems," *IEEE Transactions on Power Delivery*, vol. 17, no. 1, pp. 173-181, 2002.

[21] Z. Qin, D. Shirmohammadi, and W. H. E. Liu, "Distribution feeder reconfiguration for service restoration and load balancing," *IEEE Transactions on Power Systems*, vol. 12, no. 2, pp. 724-729, 1997.

[22] C. Chao-Shun, L. Chia-Hung, and T. Hung-Ying, "A rule-based expert system with colored Petri net models for distribution system service restoration," *IEEE Transactions on Power Systems*, vol. 17, no. 4, pp. 1073-1080, 2002.

[23] J. M. Solanki, S. Khushalani, and N. N. Schulz, "A Multi-Agent Solution to Distribution Systems Restoration," *IEEE Transactions on Power Systems*, vol. 22, no. 3, pp. 1026-1034, 2007.

[24] S. Thiébaux, C. Coffrin, H. Hijazi, and J. Slaney, "Planning with MIP for supply restoration in power distribution systems," in *Proceedings of the Twenty-Third international joint conference on Artificial Intelligence*, Beijing, China, 2013, pp. 2900-2907.

[25] D. S. Gazzana, G. D. Ferreira, A. S. Bretas, et al, "Multi-objective optimization model for distribution systems restoration." in *Proceedings of IEEE PES Innovative Smart Grid Technologies Latin America*, Montevideo, Uruguay, 2015. pp. 13-18.

[26] B. Chen, S. Mashayekh, K. L. Butler-Purry and D. Kundur, "Impact of cyber attacks on transient stability of smart grids with voltage support devices," *2013 IEEE Power & Energy Society General Meeting*, Vancouver, BC, 2013, pp. 1-5.

[27] "MIP formulations and linearizations: Quick Reference,"[Online]. Available:https://docplayer.net/53911163-Mip-formulations-and-linearizations-quick-reference.html.

[28] C. Chen, J. Wang, F. Qiu, and D. Zhao, "Resilient Distribution System by Microgrids Formation After Natural Disasters," *IEEE Transactions on Smart Grid*, vol. 7, no. 2, pp. 958-966, 2016.

[29] A. Arif, and Z. Wang, "Networked microgrids for service restoration in resilient distribution systems," *IET Generation, Transmission & Distribution*, vol. 11, no. 14, pp. 3612-3619, 2017.

[30] W. H. Kersting, *Distribution System Modeling and Analysis, Third Edition*: CRC Press, 2012.

[31] A. R. Bergen and V. Vittal, Power Systems Analysis, 2nd ed. Upper Saddle River, NJ, USA: Prentice-Hall, 1999.

[32] ANSI C84.1-2011 Electric Power Systems and Equipment - Voltage Ranges.

[33] B. A. Robbins, H. Zhu, and A. D. Domínguez-García, "Optimal Tap Setting of Voltage Regulation Transformers in Unbalanced Distribution Systems," *IEEE Transactions on Power Systems*, vol. 31, no. 1, pp. 256-267, 2016.

[34] IEEE PES Power System Analysisand Economics Committee. IEEE 123 Node Test Feeder, Feb. 2014 [Online]. Available: http://ewh.ieee.org/soc/pes/dsacom/testfeeders/feeder123.zip.

[35] N. G. Bretas, S. A. Piereti, A. S. Bretas, and A. C. P. Martins, "A Geometrical View for Multiple Gross Errors Detection, Identification, and Correction in Power System State Estimation," *IEEE Transactions on Power Systems*, vol. 28, no. 3, pp. 2128-2135, 2013.

[36] Y. Liang, K. S. Tam, and R. Broadwater, "Load Calibration and Model Validation Methodologies for Power Distribution Systems," *IEEE Transactions on Power Systems*, vol. 25, no. 3, pp. 1393-1401, 2010.

Bo Chen (M'17) received the Ph.D. degree in electrical engineering from Texas A&M University, College Station, USA, in 2017. He received the B.S. and M.S. degrees from North China Electric Power University, Baoding, China. In 2016, he worked as a research aide at the Argonne National Laboratory, IL, USA. Currently, he is a postdoctoral researcher at the Energy Systems Division, Argonne National Laboratory, IL, USA. His research interests include modeling, control, and optimization of power systems, cybersecurity, and cyber-physical systems.

Zhigang Ye (S'17) received the B.S. degrees from Xi'an Jiaotong University, Xi'an, China, in 2013, and he is currently pursuing his Ph.D. degree in the same university. He was also a visiting student at Texas A&M University, College Station, USA, during Oct. 2016 – Jul. 2017, and a visiting student at the Energy System Division, Argonne National Laboratory, IL, USA during Aug. 2017 – Oct. 2018. His research interests include modeling of power system reliability and resilience, and algorithms for bilevel mixed-integer programming.

Chen Chen (M'13) received the B.S. and M.S. degrees from Xi'an Jiaotong University, Xi'an, China, in 2006 and 2009, respectively, and the Ph.D. degree in electrical engineering from Lehigh University, Bethlehem, PA, USA, in 2013. During 2013-2015, he worked as a Postdoctoral Researcher at the Energy Systems Division, Argonne National Laboratory, Argonne, IL, USA. Dr. Chen is currently an Energy Systems Scientist with the Energy Systems Division at Argonne National Laboratory. His primary research is in optimization, communications and signal processing for smart electric power systems, power system resilience, and cyber-physical system modeling for smart grids. He is an editor of IEEE Transactions on Smart Grid and IEEE Power Engineering Letters.

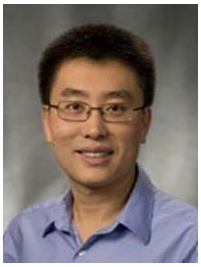

Jianhui Wang (M'07-SM'12) received the Ph.D. degree in electrical engineering from Illinois Institute of Technology, Chicago, Illinois, USA, in 2007.
Presently, he is an Associate Professor with the Department of Electrical Engineering at Southern Methodist University, Dallas, Texas, USA. Prior to joining SMU, Dr. Wang had an eleven-year stint at Argonne National Laboratory with the last appointment as Section Lead – Advanced Grid Modeling. Dr. Wang is the secretary of the IEEE Power & Energy Society (PES) Power System Operations, Planning & Economics Committee. He has held visiting positions in Europe, Australia and Hong Kong including a VELUX Visiting Professorship at the Technical University of Denmark (DTU). Dr. Wang is the Editor-in-Chief of the IEEE Transactions on Smart Grid and an IEEE PES Distinguished Lecturer. He is also the recipient of the IEEE PES Power System Operation Committee Prize Paper Award in 2015.